Ann. Geophys., 27, 2555–2563, 2009
www.ann-geophys.net/27/2555/2009/

Annales Geophysicae

Semidiurnal tidal signature in sporadic E occurrence rates derived from GPS radio occultation measurements at higher midlatitudes

C. Arras[1], **C. Jacobi**[2], **and J. Wickert**[1]

[1]Helmholtz Centre Potsdam, German Research Centre for Geosciences (GFZ), Department 1: Geodesy and Remote Sensing, Germany
[2]University of Leipzig, Institute for Meteorology, Germany

Received: 13 August 2008 – Revised: 10 June 2009 – Accepted: 10 June 2009 – Published: 24 June 2009

Abstract. GPS (Global Positioning System) Radio occultation (RO) measurements from CHAMP, GRACE and FORMOSAT-3/COSMIC satellites at Northern Hemisphere midlatitides (50°–55° N) are analysed to obtain the diurnal variation of sporadic E layer occurrence frequency in 2006 and 2007. Interconnections with zonal wind shears measured by meteor radar at Collm (51.3° N, 13° E), Germany, are investigated. According to theory, maximum E_s occurrence is expected when the zonal wind shear, which is mainly produced by the semidiurnal tide in midlatitudes, is negative. This is confirmed by the present measurements and analysis.

Keywords. Ionosphere (Ionosphere-atmosphere interactions; Mid-latitude ionosphere) – Meteorology and atmospheric dynamics (Thermospheric dynamics)

1 Introduction

Sporadic E (E_s) layers are thin sheets of enhanced electron density which appear in the lower ionospheric E region at altitudes between 90 and 120 km. They have been detected using radiowave measurements from ionosondes, incoherent scatter radars, or backscatter radars (Mathews, 1998). Available climatologies show that E_s is mainly a summer phenomenon at midlatitudes, with strong enhancement in both occurrence and intensity in May–August (e.g., Whitehead, 1989).

Recent investigations indicate, that metal ion production through meteor flux is an important factor for E_s formation at midlatitudes, since meteor rates peak during summer, which seems to explain reasonably much of the well known seasonal E_s variation (Haldoupis et al., 2007). The meteor metallic ions are accumulated into thin layers through convergence inside vertical wind shear nodes in the horizontal wind. According to the windshear theory (Whitehead, 1960), E_s layers are produced through $\mathbf{v} \times \mathbf{B}$ motions where $\mathbf{v}$ is the horizontal neutral wind velocity and $\mathbf{B}$ the intensity of the Earth's magnetic field. Neglecting diffusion and electric field forces, and taking into account that the magnetic field lines at midlatitudes are essentially directed northward, the vertical ion drift W in the E region may be written as:

$$W \approx \frac{\cos I \sin I}{1+(\frac{\nu_i}{\omega_i})^2} v + \frac{\frac{\nu_i}{\omega_i}\cos I}{1+(\frac{\nu_i}{\omega_i})^2} u \quad (1)$$

where I is the magnetic dip angle, ν_i/ω_i is the ratio of ion-neutral collision frequency to ion gyrofrequency, and u and v are the neutral horizontal winds defined geographic eastward and northward, respectively. Taking into account that $\nu_i/\omega_i \gg 1$ in the lower E region below about 115 km, the first term in Eq. (1) can be omitted. At lower E region altitudes, which are of interest in the present study, the vertical ion drift W therefore can be assumed to essentially depend on the zonal wind u. The condition for E_s formation requires a negative vertical ion convergence, that is, $(\partial W/\partial z < 0)$. For a northward and downward directed magnetic field (as in the North Hemisphere), this condition is satisfied in the presence of a negative vertical wind shear in the horizontal wind $(\partial u/\partial z < 0)$. The latter occurs when either westward (negative) zonal winds are found above eastward (positive) winds, or decreasing/increasing eastward/westward winds with altitude are prevailing.

Since the daily mean background wind shear in the midlatitude lower thermosphere is positive during summer, this may question the described origin of E_s layers. However, as summarised in Mathews (1998), the motion and variability of midlatitude E_s can be described by the semidiurnal (SDT) and diurnal tides (DT) in the lower thermosphere. This leads to the reproduction of the downward moving tidal signatures in E_s ionosonde registrations (e.g. Haldoupis et al., 2006).

Correspondence to: C. Arras
(arras@gfz-potsdam.de)

Tides are by far the strongest oscillation within lower thermosphere dynamics. The major components are the DT at lower latitudes and lower midlatitudes, and the SDT at higher midlatitudes, (e.g. Pancheva et al., 2002). The tidal amplitudes may reach values of more than 40 m/s (Manson et al., 2002a; Jacobi et al., 2009). Consequently, much stronger shears can be present compared to the background circulation, which is provided in available climatologies.

The described mechanism indicates that the negative wind shears needed to produce E_s during summer are provided by tides. Therefore the tidal signatures must be imbedded in E_s variability. As shown by Pancheva et al. (2003), also the observed correlation between E_s and planetary waves has its origin in the modulation of tides by planetary waves in the mesosphere and lower thermosphere. This confirms that the tidal wind shears shape the layers and that this is not a direct effects of planetary waves.

Taking into account that the SDT is a major dynamical feature in the midlatitude lower thermosphere, the wind shear theory indicates that a SDT oscillation should be evident in E_s occurrence. Consequently, the phases of the SDT oscillation should approximately equal the one of the neutral wind shear. This phenomenon is frequently reported to be seen in E_s registrations, but concomitant measurements of neutral atmospheric tides and E_s signatures to compare the phases are still sparse. This is mainly due to the fact that E_s layers are usually investigated using ground-based measurements, for which neutral wind data are not necessarily available in parallel.

The aim of the present study is to qualitatively investigate the correlation between tidal winds in the mesosphere-lower thermosphere and sporadic E occurrence in the northern midlatitudes. Therefore E_s occurrence rates derived from satellite based GPS RO measurements are used for the investigations as a function of local time for a latitudinal range of 50–55° N. The E_s occurrence rates are compared against local meteor radar wind shear measurements in order to investigate the correlation between these two phenomena.

2 Measurements and data analysis

Recent RO missions like the German CHAMP (Wickert et al., 2009), the U.S./German GRACE and the joint Taiwan-US FORMOSAT-3/COSMIC (Anthes et al., 2008) constellation are providing a total of ∼3000 globally distributed measurements per day. GPS radio occultation measurements from LEO (Low Earth Orbiter) satellites have already successfully been used to derive vertical profiles of ionospheric electron density (e.g., Hajj and Romans, 1998; Jakowski et al., 2002). In addition, layers of enhanced electron density in the lower ionosphere such as E_s can be identified, since they cause strong fluctuations in the GPS RO phase and signal-to-noise ratio (SNR) (Wu et al., 2005). In the ionosphere the phase and SNR scintillations can be directly related to strong electron density fluctuations. To detect E_s layers the SNR of the 50 Hz L1 occultation measurements is used. The advantage of these 50 Hz RO data, compared to the usually used 1 Hz data in ionospheric altitude, is the high vertical resolution of the derived ionospheric parameters. The upper boundary of these data is located at about 125 km altitude. Therefore it is not possible to observe sporadic E layers at higher altitudes where its formation might be influenced by the meridional wind or the descending intermediate layers. A more detailed description and initial results of the application of this technique are given by Arras et al. (2008) and Wickert et al. (2009).

The current analysis procedure provides no information on the amplitude, thickness and critical frequency of the respective E_s layer, since only the variation of the SNR for a specific occultation event at a certain time and location is measured. Furthermore, no information on the temporal behaviour of the detected layer is available, because the resolution of the RO measurements in time and space is not sufficient. But, through sorting CHAMP, GRACE and FORMOSAT-3/COSMIC data into voxels, the number of registered events is appropriate to obtain information on the mean occurrence rate or probability of E_s for each latitude, longitude, and altitude, depending on season and local time. Mean occurrence rates of E_s on a $5°\times5°$ grid with a 1 km height resolution based on data sets of 3 months each are calculated. Longitudinal means of E_s occurrence rates are computed in order to obtain a sufficient data coverage. The RO results are sorted according to local time to make the signatures of migrating tides visible in E_s. The used time intervals are centered at 4 months (October 2006, January, April and July 2007). In total 1 016 100 RO measurements are analysed, with 142,185 of them with E_s, e.g. an E_s occurrence rate of 14.0% is found on a global and annual average.

The zonal mean relative frequency of E_s occurrence for different heights and latitudes for each of the 4 seasons is depicted in Fig. 1. The figure shows the known features (e.g. Wu et al., 2005; Arras et al., 2008), e.g. that E_s is mainly a summer phenomenon at midlatitudes, with maximum rates at about 40° latitude. The values for the Southern Hemisphere are smaller than those for the Northern Hemisphere. During equinoxes, E_s layers are mainly found at lower latitudes of both hemispheres, and the probability of occurrence is lower. The smallest values are seen in Northern Hemisphere autumn. Maximum values of E_s occurrence are observed at altitudes between 100 and 105 km. Note that the E_s frequencies in Fig. 1 are given in values of 1/1000, which means that there is a relatively low probability of E_s at a given time in a given height interval. However, summing-up all E_s events at all heights in a given 5 degree latitude interval leads to E_s frequencies of up to 38.5% in summer at midlatitudes (Fig. 2).

For tidal analysis, the Collm Observatory (51.3° N, 13° E) all-sky meteor radar winds (Jacobi et al., 2007, 2009) are

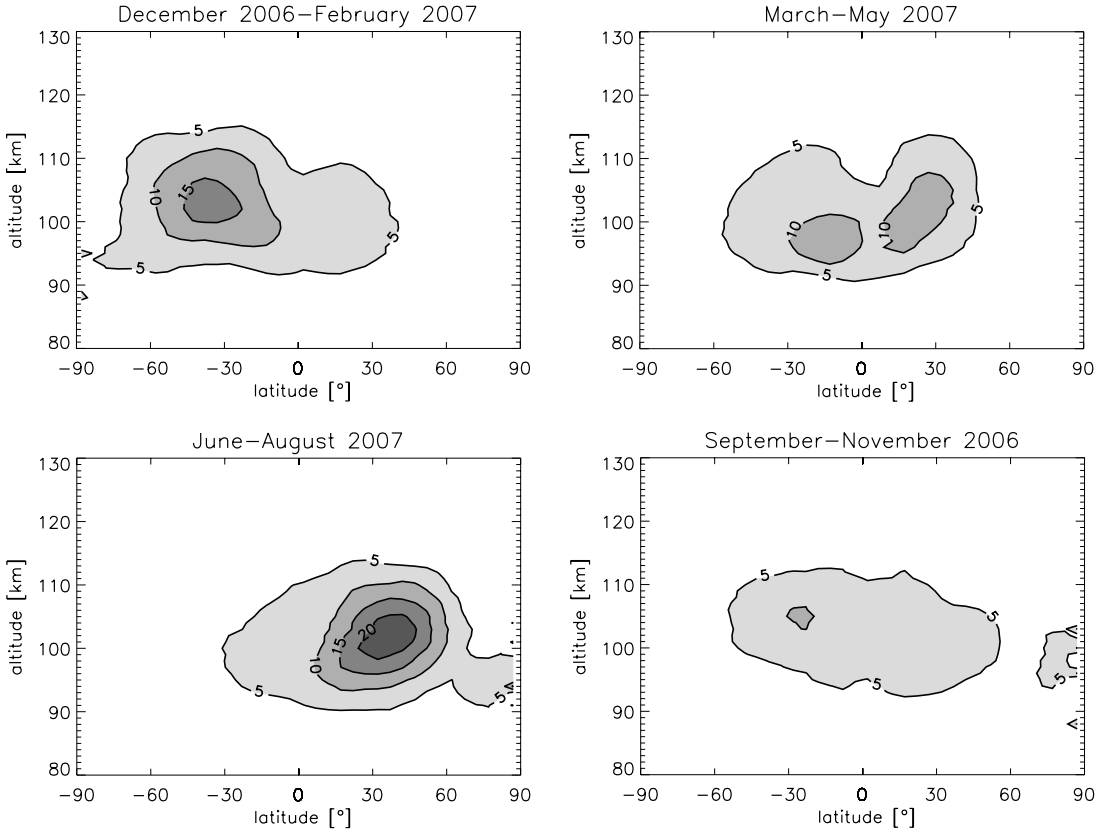

Fig. 1. Combination of CHAMP, GRACE and FORMOSAT-3/COSMIC RO mean relative E_s occurrence rate for 4 seasons (3-monthly means). Values are given in 1/1000.

used in the altitude range of 80–100 km. Individual radial winds are calculated from the Doppler shift detection of the reflected 36.2 MHz VHF radio waves from ionised meteor trails. They are collected to form hourly mean values using least squares of the horizontal wind components to raw radial wind data under the assumption that vertical winds are small (Hocking et al., 2001). The data are binned in 6 different altitude intervals centered at 82, 85, 88, 91, 94, and 98 km. In this study monthly means of hourly winds are used depending on local time during the 4 months mentioned above. The winds are shown in the upper and middle panels of Fig. 3. The SDT component is generally dominating. Monthly means of hourly zonal wind shears $s \approx \triangle u/\triangle z$ referring to the center between two adjacent height gates have been added to the panels. At times, negative zonal wind shear is visible during each month, however, in summer owing to the strong positive background vertical zonal wind gradient increase, negative values are only found in the upper layers above about 90 km altitude.

Visual inspection shows that in January and October the vertical gradients of the wind shear and the one of the wind itself are of the same order of magnitude. However, the slope of the isolines is quantitatively different, and especially in

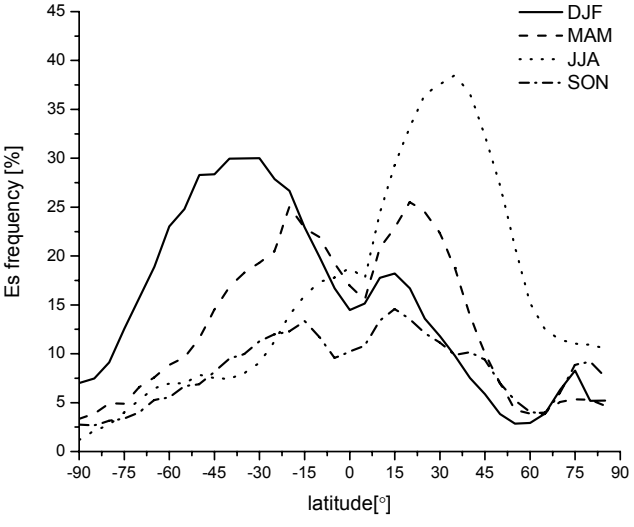

Fig. 2. Total E_s occurrence frequency in a given latitude interval, for 4 different seasons.

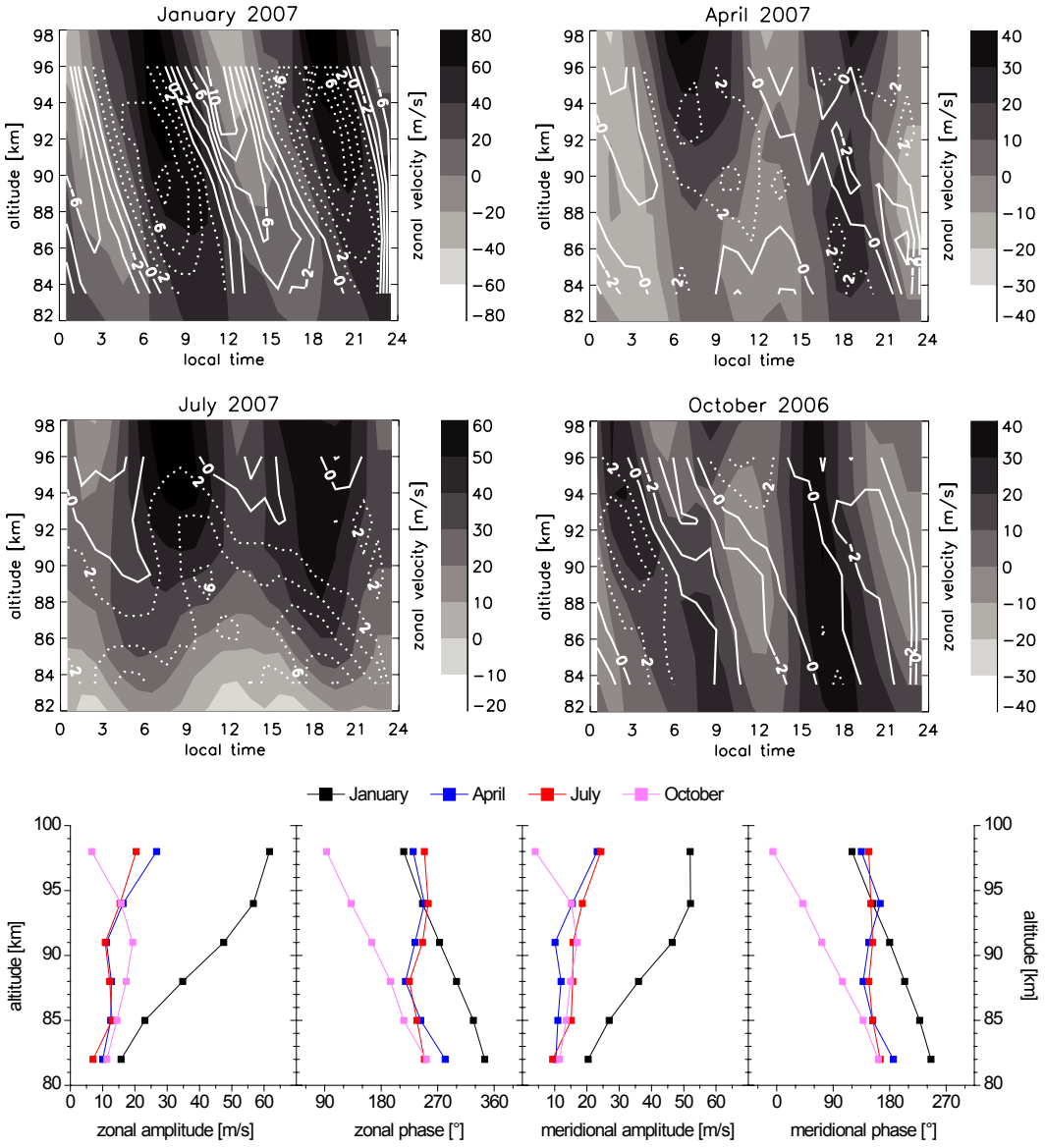

Fig. 3. Monthly mean zonal winds over Collm, for 4 seasons (color code) and vertical zonal wind shears derived from these winds (contours). Note the different scaling of the ordinate in the respective panels. In the lowermost panels amplitudes and phases of the zonal and meridional SDT are shown for 4 months. The phases refer to local midnight.

summer, where the SDT is evanescent below ∼92 km, a vertical gradient of the wind shear isolines is observed, while the wind phase is nearly constant with height.

SDT amplitudes and phases (lower panel of Fig. 3) are calculated by fitting monthly mean winds, SDT, DT and terdiurnal tidal oscillations to one month of individual hourly data for each height gate. For the sake of completeness, the meridional amplitudes and phases are also shown. As expected, the SDT components are nearly circularly polarised. Maximum amplitudes of the SDT can be found in winter. In summer, large amplitudes are visible only in the upper levels considered here. This behaviour is well known from available climatologies (e.g. Manson et al., 2002b; Kürschner and Jacobi, 2005). Vertical wavelengths derived from the phase profiles are about 40 km in January and October, but very long in April and July. The latter indicates the presence of two SDT modes, with a tendency for shorter vertical wavelengths above 90 km.

In Fig. 4 Collm meteor count rates are presented. In the upper panel, the daily meteor count rates are shown to provide an overview of the seasonal cycle. Note, however, that also the mean meteor height has a typical seasonal cycle with

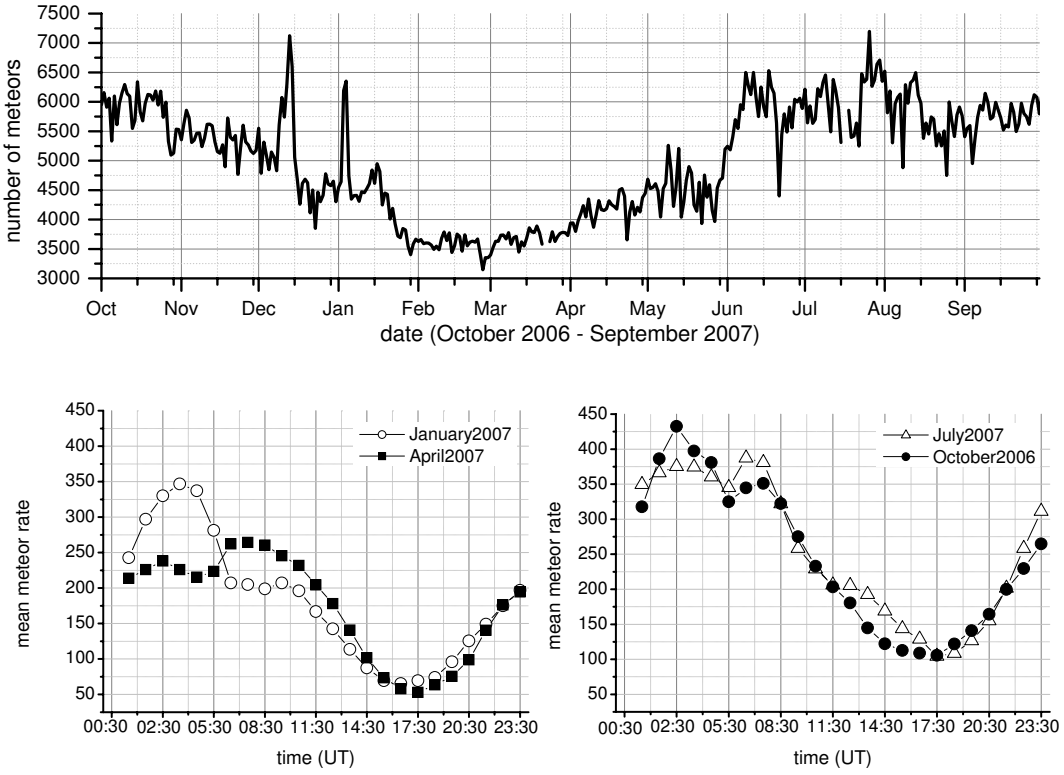

Fig. 4. Daily meteor count rates at Collm (upper panel) and monthly mean diurnal cycle of meteor count rates for four different months (lower panel).

greater heights during autumn. In addition, meteors burning at higher altitudes generally enter the Earth's atmosphere with higher velocities. The radar has a certain detection window for meteors, which is among others sensitive to meteor mass and velocity. Thus, the seasonal cycle of the detected meteors provides only a qualitative picture of the seasonal mass entry. In the lower panels of Fig. 4 the mean diurnal cycles of detected meteors are shown for 4 months. The variability shows a broad maximum in the morning, mainly due to Earth's rotation.

3 Comparison of E_s and wind shear phases over Collm

The seasonal CHAMP, GRACE and FORMOSAT-3/COSMIC E_s occurrence frequencies for the latitude range 50°–55° N are binned into hourly intervals of local time to make the correlation between zonal wind shear and E_s visible. In Fig. 5 these data are shown in colour code as a height-local time cross section for 4 seasons. Maximum values reach up to 5.6% in summer. Note that the numbers of each altitude level should be added up to obtain the total E_s occurrence frequency. During each season a descending structure of E_s probability with local time is visible. There, a clear semidiurnal pattern in E_s occurrence can be identified at about 100–105 km altitude. The zonal wind shears from Fig. 3 are shown in the lower part of the panels. The isolines of the negative wind shear values, which are required for E_s formation, are marked by solid lines. A good qualitative correspondence between negative zonal wind shear and E_s is observed in each month at upper radar altitudes around 95 km, if the wind shears would be extrapolated to higher altitudes. At first glance the highest E_s rates in summer disagree with strongest zonal wind shears found during winter. However, in addition to the vertical wind shears, the meteor rates have to be considered for the correct interpretation of this phenomenon (Haldoupis et al., 2007). Similarly to maximum E_s rates the strongest meteor incidence and therefore the most metallic ions are entering the Earth's atmosphere during summer and autumn months. Although the MLT (Mesosphere Lower Thermosphere) wind shears are weaker in summer they are, especially at altitudes above the measuring height of the meteor radar, strong enough to compress the metallic ions into thin layers. It is also noted that sporadic E layers are formed at altitudes well above the maximum altitude of the meteor radar measurements. E.g., considerable SDT amplitudes have been observed and modelled above 100 km also in summer.

A diurnal component in the E_s signatures can also be seen in Fig. 5. However, possible influences contributing to this

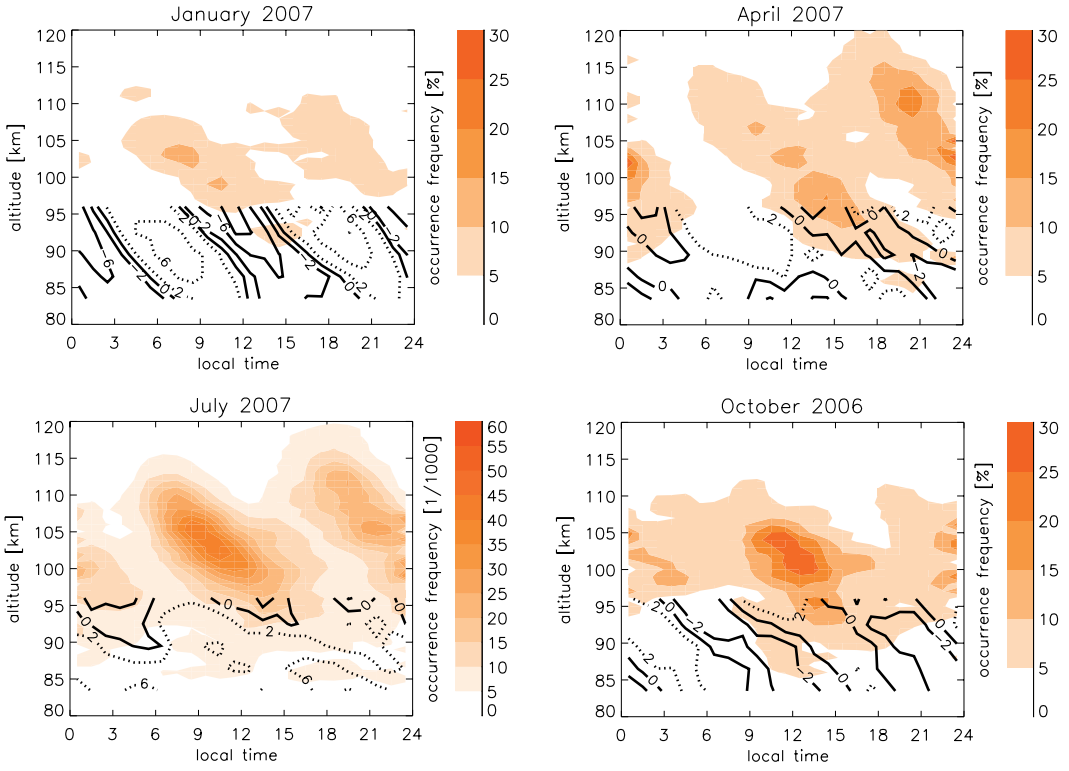

Fig. 5. CHAMP, GRACE and FORMOSAT-3/COSMIC relative E_s layer occurrence (in 1/1000), for a latitude range from 50°–55° N (redscaling). In the lower part monthly mean wind shears are shown as isolines, given in $ms^{-1}\,km^{-1}$, measured with the Collm meteor radar. Negative shear values are marked with solid isolines. Note the different scaling for summer E_s rates.

signal could be a DT in wind, increased background ionisation during daytime, and the diurnal cycle of meteor entry, which has its maximum in the early morning that would fit to the E_s phase above ∼110 km. The latter two effects are widely excluded when regarding the SDT, so that in the following this work restricts to this tide.

Figure 6 shows resulting phases of a least squares fit of a 12-h sinusoidal oscillation (referred to as a SDT oscillation) to the E_s and wind shear data. Note that the phase is defined here on the one hand as the local time of maximum E_s probability, but on the other hand, in contrast to the usual convention, as maximum negative zonal wind shear. The SDT component is practically always significant in midlatitude winds at mesopause region heights. Note that there are considerable wind amplitudes of the DT especially in spring, and that the terdiurnal tide reaches significant amplitudes in autumn (Beldon et al., 2006). Therefore, the phases shown in Fig. 6 do not exactly refer to E_s occurrence and wind shear in total, but only on their SDT component. For the semidiurnal E_s occurrence, those phase values are highlighted that are significant according to a t-test. Especially at lower altitudes and in winter, when E_s rates are low anyway, there is only a weak SDT component, which is not necessarily the dominant oscillation. Therefore, there is no clear overlapping height interval between the wind shear and E_s phase profiles in 3 of 4 seasons. However, if the wind shear phases are extrapolated linearly to larger altitudes, this again fits well to the phases in E_s. Thus, inspecting the SDT phase progression with height in both E_s and zonal negative wind shear, a clear correlation is visible even if insignificant E_s phases are included in the visual inspection (Fig. 6). Only in October at altitudes below 90 km the E_s rates are very small. Therefore, the phases do not fit to each other.

As known from theory and ground-based observations (Haldoupis et al., 2006; Christakis et al., 2009) the E_s layer descent follows the phase velocity of the SDT convergent node at altitudes well above about 100 km. Below, the descent velocity slows down due to enhanced ion-neutral collisions. In Figs. 5 and 6 this phenomenon is not clearly visible. Only in July the E_s rate slope is weakly bent below 95 km. A reason for only observing constant E_s slopes with the RO method could be that it is not possible to monitor a time series of the behaviour of a single layer. Rather Fig. 5 contains quarterly mean values of E_s occurrence in the latitude range between 50 and 55° N. Fine structures in E_s behaviour can therefore not be tracked by RO measurements. Note again that Fig. 6 does not show the track of the average E_s layers, since it shows only the SDT component detected

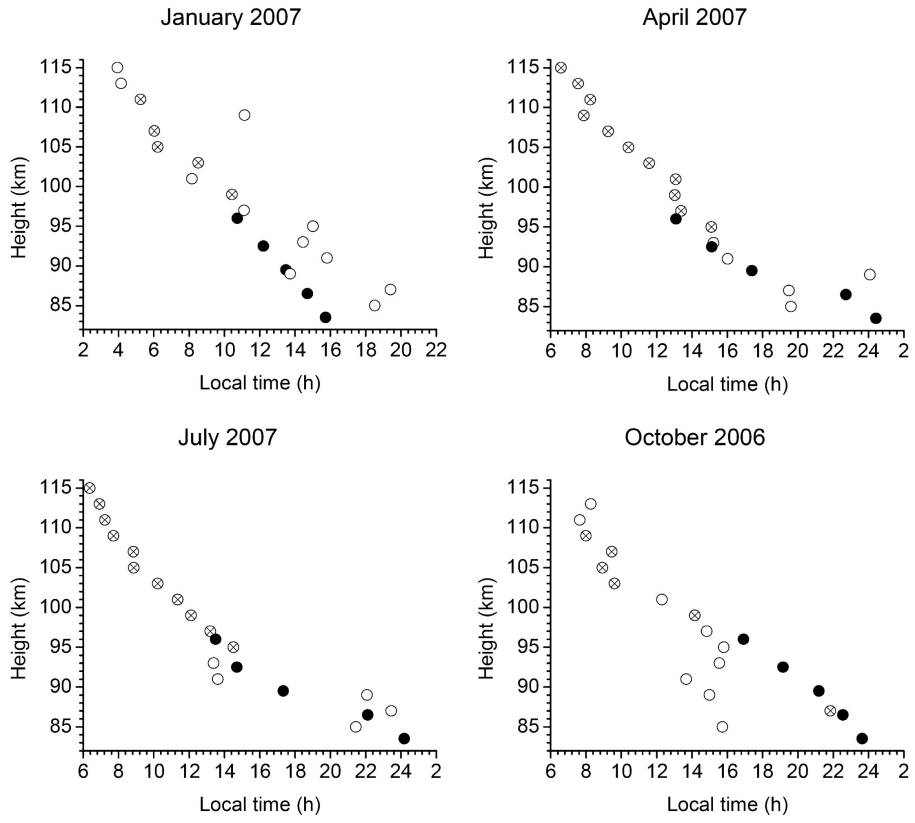

Fig. 6. Semidiurnal phases of Collm meteor radar zonal wind shear, defined as time of minimum vertical shear (solid dots), and CHAMP, GRACE and FORMOSAT-3/COSMIC relative E_s layer occurrence (open circles), defined as time of maximum occurrence. E_s phase values with statistical significant amplitudes are marked by a cross ($\times$) inside the symbol.

from a mean diurnal behaviour that is not necessarily sinusoidal. But a qualitative correspondence between the E_s and the SDT phase decent is found. The SDT component of the E_s descends above 95 km, as taken from a linear fit to the significant points in Fig. 6, at a rate of 2.2, 2.4, 2.5 and 1.5 km/h in January, April, July and October, respectively. In comparison, the SDT wind shear phase gradient is 2.5, 1.0, 1.1 and 1.8 km/h. It is noticed that during January and October, when the wind shear maximum zones descend more quickly, the E_s descend is slightly slower. This may be due to the fact that at lower altitudes formation of E_s becomes too slow to remain inside the convergence zone (Haldoupis et al., 2006). During April and July, the SDT phase gradient shows a complex picture (see Fig. 3) and the phase gradient at least below $\sim$90 km is not necessarily correlated with the one above that height. The descent speeds of both E_s and wind shear are much smaller compared to the SDT wind, which means that from the phases shown in Fig. 6 the vertical wavelength of the SDT cannot be derived. This is caused by the fact that the vertical wind shear depends not only on the wave phase, but also on the amplitude growth with height. In particular, if the SDT amplitudes decrease with altitude, as it is frequently the case in the summer half year (see Fig. 3), the wind shear phase gradient is stronger (negative) than the wind phase gradient.

4 Conclusions

A strong qualitative correlation of E_s with the SDT in zonal wind shear is shown, using the GPS RO data from CHAMP, GRACE and FORMOSAT-3/COSMIC together with Collm zonal wind shears, extrapolated to E_s altitudes. This result supports the theory that zonal wind shear plays an essential role in E_s formation at midlatitudes in the presence of metallic ions of meteoric origin. The SDT is a dominant circulation pattern in the midlatitude lower thermosphere. Consequently it is found that SDT wind shear phases are in remarkable qualitative correspondence with phases of the semidiurnal component of sporadic E variability within one day. The presented results indicate that GPS RO observations have the potential to detect the seasonal mean SDT in E_s, and thus may provide a qualitative measure on lower thermosphere dynamics at altitudes above 100 km that are not accessible to most radar systems. Since data on background ionisation

are not considered here, at this stage only conclusions on the phase of E_s occurrence can be drawn. Note, that from the phase gradient of E_s the vertical wavelength of the tide cannot be derived, because this would require knowledge of the amplitude change with height. The used detection algorithm allows for detection of an individual E_s layer, but not for derivation of information on its thickness or its absolute electron density. Since the GPS RO measurements are irregularly distributed in time and space, it is not possible to detect the evolution of E_s in time at a distinct point, but information on seasonal means or climatological behaviour of its occurrence can be derived with a high spatial resolution. The upper boundary of the used 50 Hz GPS RO data is located at around 125 km altitude. This technical limitation prohibits to observe layers higher up in the ionosphere such as descending intermediate layers.

Although the SDT is the dominant feature in the midlatitude lowermost thermosphere, the DT and even the terdiurnal tide is also present in the wind field, although with lower amplitudes in most months. However, the DT is dominating at lower latitudes, and therefore is expected to be present in the daily variations of the E_s layer strength. In addition, a terdiurnal signature should be visible where this tide is strong enough. This requires a global comparison of sporadic E and neutral dynamics using satellite winds, which will be topic of future work.

Acknowledgements. The authors thank the CHAMP and GRACE team at GFZ and JPL for their work. We acknowledge UCAR (Boulder, US) and NSPO (Taiwan) for the free and rapid provision of FORMOSAT-3/COSMIC data and related support. Part of the work, described in this paper, was funded by grant WI 2634/2-1 within the German DFG priority research program 1176 related to CAWSES.

Topical Editor K. Kauristie thanks C. Haldoupis and D. Wu for their help in evaluating this paper.

References

Anthes, R. A., Bernhardt, P. A., Chen, Y., Cucurull, L., Dymond, K. F., Ector, D., Healy, S. B., Ho, S.-P., Hunt, D. C., Kuo, Y.-H., Liu, H., Manning, K., McCormick, C., Meehan, T. K., Randel, W. J., Rocken, C., Schreiner, W. S., Sokolovskiy, S. V., Syndergaard, S., Thompson, D. C., Trenberth, K. E., Wee, T.-K., Yen, N. L., and Zeng, Z.: The COSMIC/FORMOSAT-3 Mission: Early Results, B. Am. Meteorol. Soc., 89(3), 313–333, doi:10.1175/BAMS-89-3-313, 2008.

Arras, C., Wickert, J., Jacobi, C., Heise, S., Beyerle, G., and Schmidt, T.: A global climatology of ionospheric irregularities derived from GPS radio occultation, Geophys. Res. Lett., 35, L14809, doi:10.1029/2008GL034158, 2008.

Beldon, C. L., Muller, H. G., and Mitchell, N. J.: The 8-hour tide in the mesosphere and lower thermosphere over the UK, 1988–2004, J. Atmos. Solar Terr. Phys., 86, 655–668, 2006.

Christakis, N., Haldoupis, C., Zhou, Q., and Meek, C.: Seasonal variability and descent of mid-latitude sporadic E layers at Arecibo, Ann. Geophys., 27, 923–931, 2009, http://www.ann-geophys.net/27/923/2009/.

Hajj, G. A. and Romans, L. J.: Ionospheric electron density profiles obtained with the Global Positioning System: Results from the GPS/MET experiment, Radio Sci., 33, 175–190, 1998.

Haldoupis, C., Meek, C., Christakis, N., Pancheva, D., and Bourdillon, A.: Ionogram height-time-intensity observations of descending sporadic E layers at mid-latitudes, J. Atmos. Solar Terr. Phys., 68, 539–557, 2006.

Haldoupis, C., Pancheva, D., Singer, W., Meek, C., and MacDougall, J.: An explanation for the seasonal dependence of midlatitude sporadic E layers, J. Geophys. Res., 112, A06315, doi:10.1029/2007JA012322, 2007.

Hocking, W. K., Fuller, B., and Vandepeer, B.: Real-time determination of meteor-related parameters utilizing modern digital technology, J. Atmos. Solar Terr. Phys., 63, 155–169, 2001.

Jacobi, C., Fröhlich, K., Viehweg, C., Stober, G., and Kürschner, D.: Midlatitude mesosphere/lower thermosphere meridional winds and temperatures measured with Meteor Radar, Adv. Space Res., 39, 1278–1283, 2007.

Jacobi, C., Arras, C., Kürschner, D., Singer, W., Hoffmann, P., and Keuer, D.: Comparison of mesopause region meteor radar winds, medium frequency radar winds and low frequency drifts over Germany, Adv. Space Res., 43, 247–252, 2009.

Jakowski, N., Wehrenpfennig, A., Heise, S., Reigber, C., Lühr, H., Grunwaldt, L., and Meehan, T. K.: GPS radio occultation measurements of the ionosphere from CHAMP: early results, Geophys. Res. Lett., 29(10), 1457, doi:10.1029/2001GL014364, 2002.

Kürschner, D. and Jacobi, C.: The mesopause region wind field over Central Europe in 2003 and comparison with a long-term climatology, Adv. Space Res., 35, 1981–1986, 2005.

Manson, A. H., Luo, Y., and Meek, C.: Global distributions of diurnal and semi-diurnal tides: observations from HRDI-UARS of the MLT region, Ann. Geophys., 20, 1877–1890, 2002a.

Manson, A. H., Meek, C., Hagan, M., Koshyk, J., Franke, S., Fritts, D., Hall, C., Hocking, W., Igarashi, K., MacDougall, J., Riggin, D., and Vincent, R.: Seasonal variations of the semi-diurnal and diurnal tides in the MLT: multi-year MF radar observations from 2–70° N, modelled tides (GSWM, CMAM), Ann. Geophys., 20, 661–677, 2002b.

Mathews, J. D.: Sporadic E: current views and recent progress, J. Atmos. Sol. Terr. Phys., 60, 413–435, 1998.

Pancheva, D., Merzlyakov, E., Mitchell, N. J., Portnyagin, Y., Manson, A. H., Jacobi, C., Meek, C. E., Luo, Y., Clark, R. R., Hocking, W. K., MacDougall, J., Muller, H. G., Kürschner, D., Jones, G. O. L., Vincent, R. A., Reid, I. M., Singer, W., Igarashi, K., Fraser, G. I., Fahrutdinova, A. N., Stephanov, A. M., Poole, L. M. G., Malinga, S. B., Kashcheyev, B. L., and Oleynikov, A. N.: Global-scale tidal variability during the PSMOS campaign of June–August 1999: interaction with planetary waves, J. Atmos. Solar Terr. Phys., 64, 1865–1896, 2002.

Pancheva, D., Haldoupis, C., Meek, C. E., Manson, A. H., and Mitchell, N. J.: Evidence of a role for modulated atmospheric tides in the dependence of sporadic E layers on planetary waves, J. Geophys. Res., 108(A5), 1176, doi:10.1029/2002JA009788, 2003.

Whitehead, J.: Recent work on mid-latitude and equatorial sporadic-E, J. Atmos. Terr. Phys., 51, 401–424, 1989.

Whitehead, J. D.: Formation of the sporadic E layer in the temperate zones, Nature, 188, 567–567, 1960.

Wickert, J., Michalak, G., Schmidt, T., Beyerle, G., Cheng, C. Z., Healy, S. B., Heise, S., Huang, C. Y., Jakowski, N., Köhler, W., Mayer, C., Offiler, D., Ozawa, E., Pavelyev, A. G., Rothacher, M., Tapley, B., and Arras, C.: GPS radio occulation: Results from CHAMP, GRACE and FORMOSAT-3/COSMIC, Terr. Atmos. Oceanic Sci., 20(1), 35–50, doi:10.3319/TAO.2007.12.26.01(F3C), 2009.

Wu, D. L., Ao, C. O., Hajj, G. A., de la Torre Juarez, M., and Mannucci, A. J.: Sporadic E morphology from GPS-CHAMP radio occultation, J. Geophys. Res., 110, A01306, doi:10.1029/2004JA010701, 2005.